ACS APPLIED MATERIALS & INTERFACES

www.acsami.org
Research Article

In Vitro Photoselective Gene Transfection of Hepatocellular Carcinoma Cells with Hypericin Lipopolyplexes

Hirva Shah,[‡] Sebastian Schlüter,[‡] Muhammad Umair Amin,[‡] Alice Abu Dayyih, Konrad H. Engelhardt, Shashank Reddy Pinnapireddy, Eduard Preis,* and Udo Bakowsky*

Cite This: ACS Appl. Mater. Interfaces 2024, 16, 43416−43429
Read Online

ACCESS | Metrics & More | Article Recommendations | Supporting Information

ABSTRACT: The lipopolyplex, a multicomponent nonviral gene carrier, generally demonstrates superior colloidal stability, reduced cytotoxicity, and high transfection efficiency. In this study, a new concept, photochemical reaction-induced transfection, using photosensitizer (PS)-loaded lipopolyplexes was applied, which led to enhanced transfection and cytotoxic effects by photoexcitation of the photosensitizer. Hypericin, a hydrophobic photosensitizer, was encapsulated in the lipid bilayer of liposomes. The preformed nanosized hypericin liposomes enclosed the linear polyethylenimine (lPEI)/pDNA polyplexes, resulting in the formation of hypericin lipopolyplexes (Hy-LPP). The diameters of Hy-LPP containing 50 nM hypericin and 0.25 μg of pDNA were 185.6 ± 7.74 nm and 230.2 ± 4.60 nm, respectively, measured by dynamic light scattering (DLS) and atomic force microscopy (AFM). Gel electrophoresis confirmed the encapsulation of hypericin and pDNA in lipopolyplexes. Furthermore, in vitro irradiation of intracellular Hy-LPP at radiant exposures of 200, 600, and 1000 mJ/cm^2 was evaluated. It demonstrated 60- to 75-fold higher in vitro luciferase expression than that in nonirradiated cells. The lactate dehydrogenase (LDH) assay supported that reduced transfection was a consequence of photocytotoxicity. The developed photosensitizer-loaded lipopolyplexes improved the transfection efficiency of an exogenous gene or induced photocytotoxicity; however, the frontier lies in the applied photochemical dose. The light-triggered photoexcitation of intracellular hypericin resulted in the generation of reactive oxygen species (ROS), leading to photoselective transfection in HepG2 cells. It was concluded that the two codelivered therapeutics resulted in enhanced transfection and a photodynamic effect by tuning the applied photochemical dose.

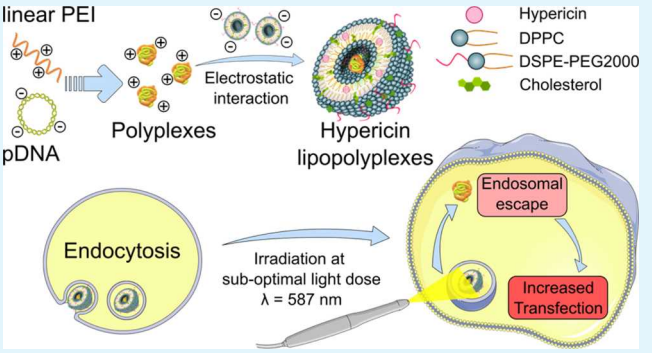

KEYWORDS: *lipopolyplexes, photosensitizer, co-encapsulation, light-sensitive transfection, gene delivery*

1. INTRODUCTION

Various biogenic macromolecules are currently under development for therapeutic purposes, with some already approved for use as vaccines and anticancer treatments. Among these, oligonucleotides (ODNs), DNA and mRNA, ribozymes, peptide nucleic acids, and siRNA have demonstrated significant therapeutic potential.[1−4] However, achieving gene delivery at the target site is highly challenging because of the physicochemical properties of these biogenic macromolecules, such as their large size, negative surface charge, and aqueous or enzymatic instability.[5] Photochemical internalization (PCI) is a promising method for improving drug and gene delivery in many diseases, including solid tumors.[6] First developed in 1999, the PCI technique is used to enhance the release of macromolecules, including peptides, protein toxins, genes, and small molecules via a photochemical reaction of a photosensitizer (PS) from endosomes and lysosomes within targeted cancer cells, allowing them to reach the cytosol where they can exert their therapeutic effects more effectively.[1,7] When irradiated at a specific wavelength, the PS absorbs energy, undergoes excitation, and releases reactive oxygen species (ROS) via a type I or type II photoreaction while returning to the ground state. If the generated ROS do not provoke cell damage in the form of photodynamic therapy (PDT), they enhance the cytosolic release of therapeutics from endosomes and lysosomes.[8,9] This light-triggered ROS generation in the intracellular compartments has attracted intense interest because of its tissue- or organ-specific gene delivery through localized laser treatment. Although it improves the effectiveness and safety of the procedure, only a few macromolecules such as gelonin, the p53 gene with glucosylated PEI, and the nuclear-localizing sequence-peptide (NLS-peptide)/plasmid complex have been studied for in vivo efficacy. Recently,

Received: June 24, 2024
Revised: July 9, 2024
Accepted: July 12, 2024
Published: August 9, 2024

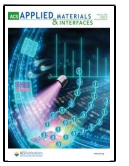

accelerated gene knockdown by RNA interference was reported in an in vivo murine melanoma model, demonstrating the enormous clinical potential of this system.[10,11] It emphasizes that the in vivo application of PCI for nucleic acids has remained limited because of the lack of a suitable delivery platform.[6,12] Earlier, PCI technology involved pretreatment with free PS followed by the addition of a complex illumination process. A clinical study involving the PCI method reported the pretreatment with the free photosensitizer TPCS2a, Amphinex, as a prerequisite for the photosensitizer to localize in intracellular vesicles before the illumination process.[13,14] A correct wavelength, optimal radiant exposure, PS concentration, presence of molecular oxygen, and the interval between administration and illumination (i.e., cell incubation interval) are tunable factors for efficient PCI.[15] Hypericin, a natural PS found in *Hypericum perforatum* L., exhibits excellent photodynamic properties, i.e., a high singlet oxygen quantum yield upon illumination along with minimal dark toxicity.[15−17] Recently, photosensitizers have been codelivered with therapeutic oligonucleotides for greater efficiency. A phase I clinical study with fimaVacc, a peptide- and protein-based vaccine formulated with fimaporfin, a photosensitizing compound, strongly enhanced both cellular and humoral immune responses and improved the antitumor effect in mouse models.[18] The impact of codelivered hypericin for PCI of a nucleic acid to potentiate the in vitro transfection efficiency of the nonviral vector has not been investigated until now.

Lipopolyplexes are well-established nonviral carriers for the in vivo delivery of genetic materials. We have developed lipopolyplexes incorporating linear polyethylenimine (lPEI, 22 kDa) and pDNA, which demonstrated higher transfection efficiency than polyplexes.[19,20] With recent developments in nonviral gene delivery systems, the surface modification of nanocarriers by polyethylene glycol (PEG) has attracted attention because it reduces the uptake by the in vivo reticuloendothelial system (RES). However, PEGylation of the nanocarrier prolongs its circulation time and interferes with its cellular uptake and endosomal escape capabilities (also known as the PEG dilemma). The emergence of suitable photochemical internalization for a multicellular tumor like advanced hepatocellular carcinoma is desirable.[21,22] Hereby, the co-encapsulation of hypericin and pDNA in the nanocarrier is proposed to deliver the photosensitizer and nucleic acid in cancer cells simultaneously.[23,24] This work focuses on the preparation of hypericin lipopolyplexes (Hy-LPP) to improve the transfection efficiency upon irradiation of hepatocellular carcinoma cells (HepG2) at λ_{587} nm (also known as the "light after" strategy).

2. EXPERIMENTAL SECTION

2.1. Materials. Linear polyethylenimine (lPEI; 22 kDa) was purchased from Polysciences (Eppelheim, Germany). The lPEI solution (1 mg/mL) was prepared by diluting it in ultrapure water and then adjusting to pH 7.0. 1,2-Dipalmitoyl-*sn*-glycero-3-phosphocholine (DPPC) and 1,2-distearoyl-*sn*-glycero-3-phosphoethanolamine-*N*-[methoxy (polyethylene glycol) 2000] (DSPE-PEG2000) were purchased from Lipoid GmbH (Ludwigshafen, Germany). Stock solutions of lipids were prepared in a mixture of chloroform:methanol (2:1, v/v) and stored at 4 °C. Hypericin and SYBR DNA stains were purchased from Thermo Fisher Scientific (Karlsruhe, Germany). A stock solution of hypericin was prepared in methanol and stored at 4 °C. 3-(4,5-dimethylthiazol-2yl)-2,5-diphenyltetrazolium bromide (MTT) and 2′,7′-dichlorodihydrofluorescein diacetate (H2DCFDA) were obtained from Sigma-Aldrich Chemie GmbH (Taufkirchen, Germany). The Bright-Glo Luciferase Assay System for detecting luciferase expression was purchased from Promega (Mannheim, Germany). The plasmids used for this work, pCMV-Luc and pCMV-GFP, were purchased from Plasmid Factory (Bielefeld, Germany).

2.2. Cell Culture and Harvesting Methods. The HepG2 cell line was purchased from the American Type Culture Collection (ATCC, HB-8065, Manassas). HepG2 cell lines were cultivated at 37 °C and 7% CO_2 under humid conditions in Roswell Park Memorial Institute (RPMI-1640) medium (Biochrom, Berlin, Germany) supplemented with 10% fetal calf serum (FCS) (PAA Laboratories, Cölbe, Germany). No antibiotics were used in the cell culture medium. Cells were grown as monolayers and passaged upon reaching 80% confluency.

2.3. Preparation of Hypericin Liposomes (HyLs). Hypericin liposomes (HyLs) were prepared using an ethanol injection method. Briefly, a homogeneous mixture of lipids and hypericin, having a definite concentration as shown in Table 1, was evaporated at 40 ± 2 °C under vacuum using a rotary evaporator (Laborota 4000, Heidolph Instruments, Schwabach, Germany). The resultant photosensitizer-loaded lipid film was dissolved in 200 μL of a ethanol:water mixture (9:1 v/v) and then instilled in HEPES buffer (20 mM, pH 7.4). HyLs were formed by continuous stirring using a magnetic stirrer. The remaining ethanol was evaporated using a rotary evaporator at 60 °C and 175 mbar, and aqueous buffer was added to obtain 100 μg/mL HyLs. The formulations were evaluated for their average particle size, ζ-potential, encapsulation efficiency (EE), and storage stability.

Table 1. Particle Size (Hydrodynamic Diameter), Polydispersity Index (PDI), and ζ-Potential of Hypericin Liposomes Composed of DPPC:CH:DSPE-PEG2000 (84:15:1)

hypericin concentration (nM)	average particle size (nm ± SD)	ζ-potential (mV ± SD)	PDI (±SD)
	115.5 ± 9.22	−14.3 ± 2.60	0.19 ± 0.01
50 nM	187.8 ± 14.01	−19.4 ± 2.17	0.17 ± 0.01
100 nM	177.4 ± 12.30	−18.7 ± 1.18	0.25 ± 0.02
200 nM	196.5 ± 10.21	−18.9 ± 3.32	0.26 ± 0.04
500 nM	229.0 ± 8.20	−25.6 ± 2.74	0.21 ± 0.02
1 μM	198.5 ± 6.26	−31.2 ± 5.60	0.23 ± 0.02

2.4. Preparation of Hypericin Lipopolyplexes (Hy-LPP). Hy-LPP were prepared using polyplexes at an N/P ratio of 10 and HyLs (50−500 nM hypericin) at different lipid:lPEI mass ratios using a method described elsewhere.[20] Briefly, linear polyethylenimine (lPEI) was added to pDNA, mixed, and incubated at room temperature for 20 min. Then, an appropriate amount of HyL was added to the polyplexes at different lipid:lPEI mass ratios and further incubated at room temperature for 1 h.

2.5. Physicochemical Characterization. *2.5.1. Encapsulation Efficiency.* The free hypericin from the hypericin liposome dispersion was separated by gel filtration chromatography on a PD-10 column (GE Healthcare Life Sciences).[16] The eluent was monitored by measuring the hypericin absorbance at λ_{max} = 590 nm using a UV/vis-spectrophotometer (Thermo Scientific Multiskan GO Microplate Spectrophotometer). The fraction containing HyL was collected and quantified. The percentage encapsulation efficiency (EE) was calculated using eq 1.

$$\%\ \mathrm{EE} = \frac{\text{amount of hypericin in seperated liposomes}}{\text{total amount of hypericin added into liposomes}} \times 100\% \quad (1)$$

2.5.2. Average Particle Size and ζ-Potential. The particle size (hydrodynamic diameter), size distribution, and ζ-potential were determined by dynamic light scattering (DLS) and electrophoretic light scattering (ELS) using a Zetasizer Nano ZS (Malvern Panalytical

https://doi.org/10.1021/acsami.4c10438
ACS Appl. Mater. Interfaces 2024, 16, 43416−43429

GmbH, Kassel, Germany).[25] The samples were diluted 1:9 (v/v) with ultrapure water and placed in a cuvette at 25 °C. A 4 mW HeNe laser at 633 nm was used as a light source to illuminate the sample particles within the cuvette. The scattered light was detected at an angle of 173°. The ζ-potential was determined at a scattering angle of 17° by measuring electrophoretic mobility using laser Doppler velocimetry on the same instrument. The results were calculated using data from three independent samples.

2.5.3. Atomic Force Microscopy (AFM). Atomic force microscopy was performed using a NanoWizard 3 NanoScience AFM (JPK Instruments/Bruker, Berlin, Germany). Imaging of empty liposomes (ELs), HyLs, and Hy-LPP was performed in AC mode in the air with a scanning area of 1 μm × 1 μm (512 × 512 pixels).[26] 20 μL of the sample was deposited onto a freshly cleaved silicon wafer glued onto a microscopic glass slide and incubated for 20 min to allow particle adsorption. A commercial AFM cantilever HQ:NSC14 AI BS (MikroMasch, Wetzlar, Germany) with a length of 125 μm, a resonance frequency of 160 kHz, and a force constant of 5 N/m was used for the measurements. Raw images were processed using JPK data processing software. A polynomial fit was subtracted from each scan line to flatten the images, and minor noise was corrected by applying a Gaussian low-pass filter.

2.5.4. Transmission Electron Microscopy (TEM). The structure of the formulation was analyzed via transmission electron microscopy (TEM), as described elsewhere.[27] Briefly, 6 μL of liposomes (50 μg/mL) was placed on mesh carbon grids, and the excess of the formulation was removed by filter paper. A drop of a 2% (w/v) aqueous solution of uranyl acetate was added and the sample was left in contact with the sample for 5 min. The sample was dried at room temperature and imaged with TEM operating at an accelerating voltage of 300 kV (TEM JEOL 3010, 300 kV).

2.5.5. Gel Retardation Assay. Agarose gel electrophoresis was performed to optimize the N/P ratio for lPEI/pDNA (polyplexes).[28] Briefly, 1% agarose gel containing SYBR DNA stain was prepared in TAE buffer (1×). The wells were cast on a gel using an 8-well comb. Different polyplexes containing 0.5 μg of pDNA were added to each 5 mm lane along with loading buffer containing cyan/orange dye (Invitrogen, Thermo Fischer Scientific). The gel was electrophoresed at +80 V for 1 h. DNA migration was observed under a UV transilluminator (BioDoc Analyze, Biometra) and compared with controls, which were free pDNA and DNA ladder (TrackIt DNA ladder, Invitrogen Thermo Fischer Scientific).

2.5.6. SYBR Quenching Assay. The intercalation of pDNA into polyplexes and hypericin lipopolyplexes was assessed using the SYBR quenching assay. In this method, Hy-LPP was prepared and incubated with 15 μL of SYBR solution (1×) in a white opaque bottom 96-well plate and incubated in the dark for 10 min followed by observation of the emitted fluorescence at excitation/emission wavelengths of 485/520 nm using a microplate reader (FLUOStar Optima, BMG Labtech GmbH, Offenburg, Germany). The relative quenching was calculated using eq 2.

$$F_r = \frac{F_{obs} - F_d}{F_o - F_d} \times 100\% \quad (2)$$

where F_r is the relative fluorescence, F_{obs} is the observed fluorescence, F_d is the fluorescence of the SYBR DNA dye, and F_o is the initial fluorescence of free nucleic acid.

2.5.7. Photostability. Twenty-five microliters of hypericin lipopolyplexes containing 0.5 μg of pDNA and different hypericin concentrations (50−500 nM) were prepared. Each formulation was irradiated (λ_{irr} = 587 nm) at a dose of 600 mJ/cm^2. Each formulation was irradiated and lysed using the lysis buffer as a control group.[29] The nonlysed and lysed formulations were electrophoresed using agarose gel, as described in Section 2.5.5. For lysis of the formulation, 10 μL of 0.1% SDS was added to hypericin lipopolyplexes and vortexed for 2 min, followed by incubation for 15 min before loading into the gel.

2.6. Cell Culture Experiments. *2.6.1. Cell Viability.* Cell viability was determined using the MTT assay, as described elsewhere with slight modifications.[30] 10,000 cells/well were seeded and incubated for 24 h, followed by treatment with hypericin formulations for 4 h and exposure to light. For the irradiation experiments, a prototype low-power light-emitting diode (λ_{irr} = 587 nm; Lumundus, Eisenach, Germany), custom-made to irradiate 96-well plates, providing an irradiance of 27 W/m^2 at 587 nm, was used. The cells were exposed to different radiant exposures, i.e., 200, 400, 600, and 1000 mJ/cm^2. All of the well plates were incubated for 24 h. MTT assay was performed as previously described. Briefly, the medium was aspirated, and the cells were treated with 0.5 mg/mL MTT reagent in RPMI medium (1:10). The cells were incubated for 4 h, followed by replacement of the MTT reagent with DMSO to solubilize the formazan crystals. The plates were shaken for 15 min at 150 rpm, and the absorbance was measured at 570 nm. The cells treated with 0.1% Triton-X100 served as positive controls. The experiment was performed in triplicate, and the average was considered as the mean absorbance ± SD.

2.6.2. Phototransfection. Briefly, hepatocellular carcinoma cells (HepG2, ATCC HB-8065) were seeded at a cell density of 10,000 cells/well in a sterile 96-well microtiter plate with an opaque bottom. The cells were transfected with free plasmids, polyplexes, lipopolyplexes, and hypericin lipopolyplexes. All formulations were prepared at an optimized ratio (N/P = 10 and lipid:lPEI mass ratio = 0.45) containing 0.25 μg of pCMV-Luc. The cells were incubated with the formulations in 75 μL fresh cell culture medium for 2 h. After incubation, the plates were irradiated (λ_{irr} = 587 nm) with 200, 600, and 1000 mJ/cm^2 or kept in the dark as the control. The wells were then filled with the remaining 25 μL of medium and incubated for 48 h before the subsequent assay. 100 μL of Bright-Glo luciferase assay reagent was added to the culture medium. The plate was shaken for 2 min at 200 rpm for complete lysis, followed by immediate luminescence measurement with a microplate reader (FLUOStar Optima, BMG Labtech GmbH). The cells were transfected in triplicate in each group, and the mean luminescence value ± SD was considered.

2.6.3. Photocytotoxicity. Cytotoxicity was studied upstream to evaluate transfection efficiency using a lactate dehydrogenase (LDH) Roche Kit. The cells were transfected and irradiated, as described in Section 2.6.2. After 48 h of incubation, 100 μL of the cell culture medium from the assay plates was carefully transferred to a 96-well plate with an optically transparent bottom. Further, 100 μL of freshly prepared LDH assay buffer containing WST-1, a substrate of lactate dehydrogenase, was added, and the mixture was incubated for 30 min at room temperature. The absorbance of the orange complex formed by the reaction was measured at 485 nm using a microplate reader (FLUOStar Optima, BMG Labtech GmbH). The cells treated with 10 μL of cell lysis solution were used as positive controls. The experiment was carried out in triplicate, and the mean absorbance ± SD was considered. The percentage cytotoxicity was calculated using eq 3.

$$\%\ \text{cytotoxcity} = \frac{[OD_{485}(\text{transfected cells}) - OD_{485}(\text{non-transfectected cells})]}{[OD_{485}(\text{lysed cells}) - OD_{485}(\text{non-transfectected cells})]} \times 100\% \quad (3)$$

2.6.4. Cellular Uptake with F-Actin Staining. HepG2 cells were seeded in 24-well plates containing coverslips and incubated overnight to reach the required confluence. The next day, cells were treated with free hypericin (free Hy) dissolved in DMSO, hypericin liposomes (HyLs), and hypericin lipopolyplexes (Hy-LPPs) at a final concentration of 3 μM. After different time intervals (1, 2, 4, 6, and 24 h), cells were washed twice with PBS buffer and fixed with 4% paraformaldehyde for 15 min. Following fixation, the cells were washed twice and permeabilized with 0.1% Triton-X100. The cells were washed again with chilled PBS buffer before being incubated with Phalloidin 488 for 30 min. Then, the cells were washed again with PBS buffer and stained with DAPI for 15 min. Finally, the coverslips were mounted onto glass slides using FluoroSave and

https://doi.org/10.1021/acsami.4c10438
ACS Appl. Mater. Interfaces 2024, 16, 43416−43429

Scheme 1. Preparation of Hypericin Lipopolyplexes[a]

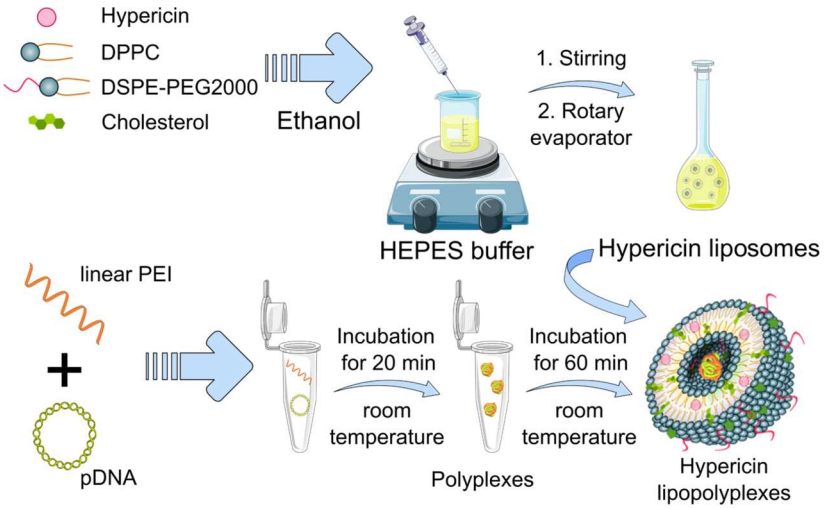

[a]lPEI in HEPES buffer was added to a pDNA aliquot and incubated for 20 min. The preformed hypericin liposomes were added to the polyplexes and incubated for 60 min. The hypericin liposomes prepared using the ethanol injection method contained different hypericin concentrations. The figure was partly generated using Servier Medical Art, provided by Servier, licensed under a Creative Commons Attribution 3.0 unported license.

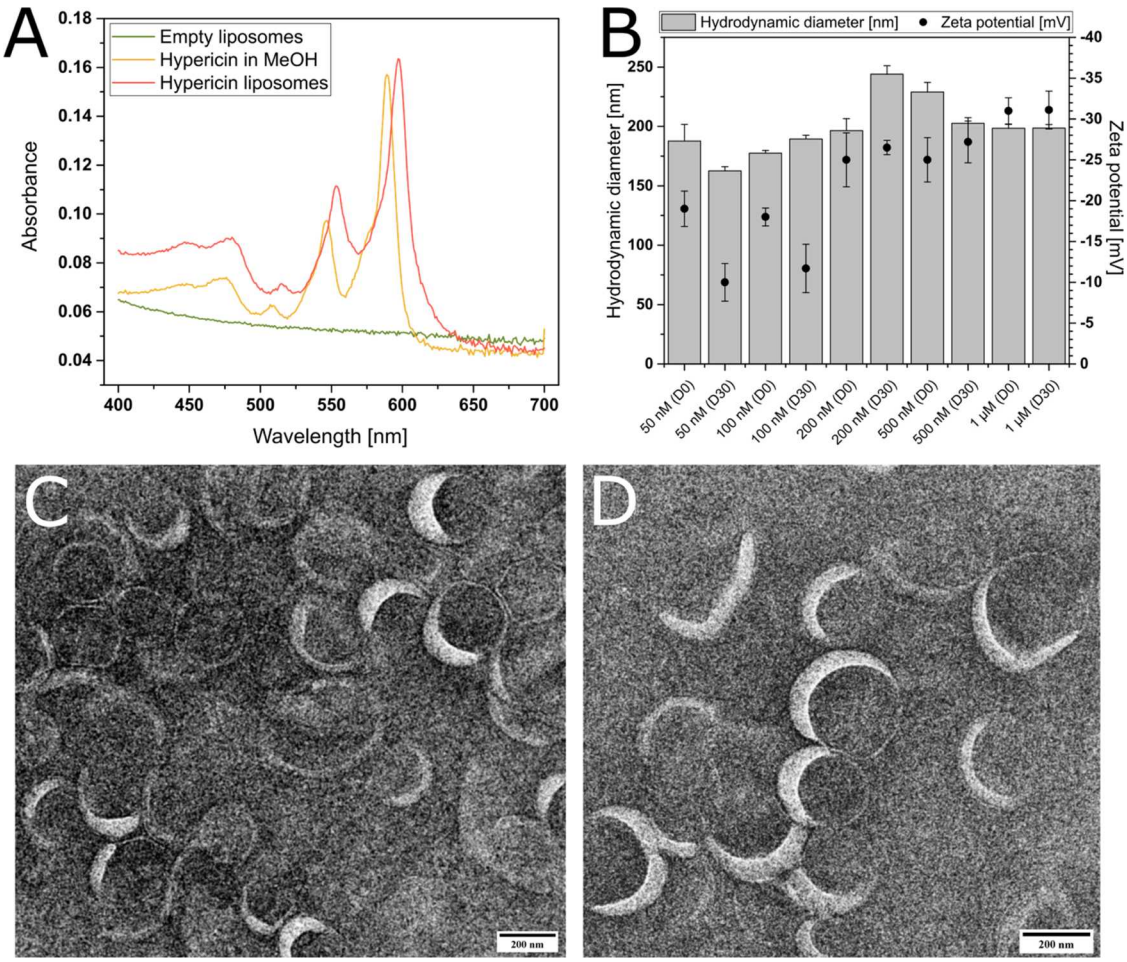

Figure 1. (A) UV/vis absorbance spectra of 1 μM free hypericin dissolved in methanol, hypericin liposomes (1 μM hypericin), and empty liposomes in 10 nM HEPES buffer. (B) Effect of storage at +4 °C for 30 days on the average particle size and ζ-potential of hypericin liposomes. The data are shown as the mean ± SD (n = 3). TEM images of (C) empty liposomes and (D) hypericin liposomes (200 nM hypericin). Scale bars represent 200 nm.

observed using a confocal laser scanning microscope (Zeiss LSM700, Carl Zeiss Microscopy GmbH, Jena, Germany). DAPI, Hy, and Phalloidin 488 (F-actin staining) were excited using 405, 488, and 555 nm lasers, respectively. The emission of DAPI and Phalloidin 488 was

https://doi.org/10.1021/acsami.4c10438
ACS Appl. Mater. Interfaces 2024, 16, 43416−43429

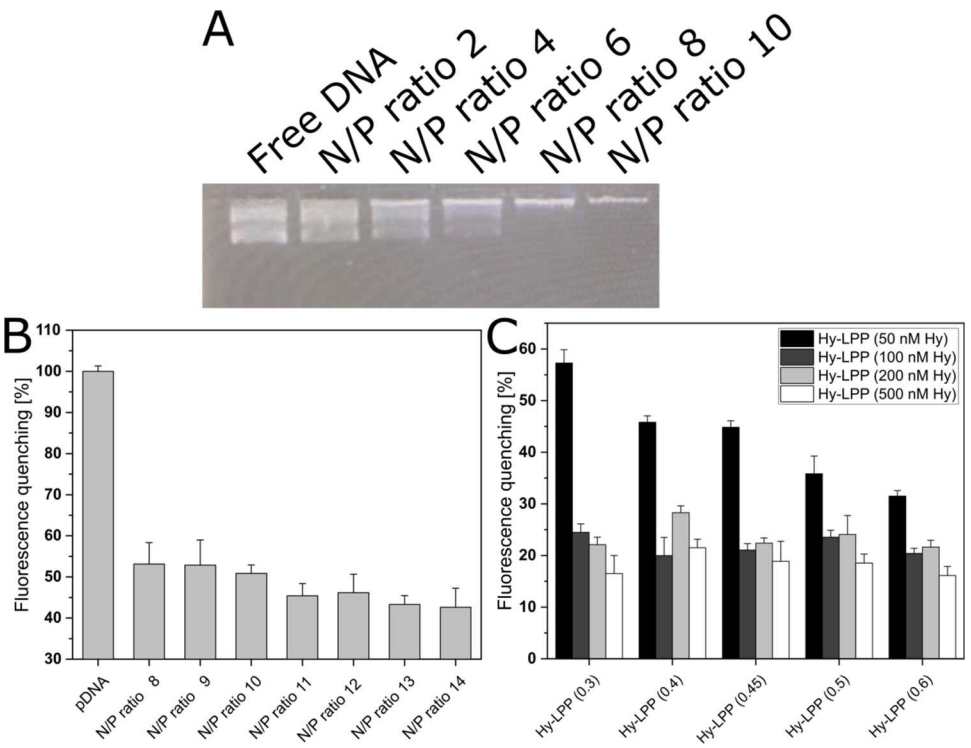

Figure 2. (A) DNA migration assay using agarose gel-electrophoresis to evaluate the degree of complexation of lPEI/pDNA polyplexes. The polyplexes were prepared with an N/P ratio of 2−10 and compared with free DNA, (B) fluorescence quenching assay for polyplexes at an N/P ratio of 8−14, and (C) fluorescence quenching assay for hypericin lipopolyplexes (Hy-LPP) at lipid:PEI mass ratios between 0.3 and 0.6 and hypericin concentrations from 50 to 500 nM. Data are shown as mean ± SD (n = 3).

detected using 490 and 555 nm short-pass filters, respectively. Hy was detected with a 560 nm long-pass filter.

2.6.5. Assessment of Cellular Distribution after Irradiation. Briefly, 24-well plates containing sterile coverslips were seeded at a cell density of 80,000 cells/well and incubated overnight. Hypericin lipopolyplexes containing 1 μg of pDNA and 50 nM hypericin were incubated for 2 h. Afterward, the cells were irradiated at 200, 600, and 1000 mJ/cm^2, and the effects of irradiation were assessed. The cells were then washed with PBS and fixed with 4% paraformaldehyde at room temperature for 15 min. The cells were counterstained with DAPI (0.6 μg/mL) in the dark at room temperature for 20 min. The coverslips were mounted on slides using FluorSave. The cells were observed using a confocal laser scanning microscope (Zeiss LSM700, Carl Zeiss Microscopy GmbH, Jena, Germany) at excitation and emission wavelengths of 590 and 620 nm for hypericin and 358 and 461 nm for DAPI visualization.

2.6.6. Detection of Cellular ROS Generation after Irradiation. The cell-permeant nonfluorescent reagent 2′,7′-dichlorodihydrofluorescein acetate (DCFDA) was used for the measurement of cellular reactive oxygen species, where on intracellular oxidation, it was converted to green fluorescent DCF (2′,7′-dichlorfluorescein).[31] Briefly, 20,000 cells/well were incubated at 37 °C overnight. After incubation, the cells were treated with 25 μL of hypericin lipopolyplexes containing 0.25 μg of pCMV-Luc per well, and 75 μL of RPMI medium was added and incubated for 2 h. The cells were further washed and incubated for 45 min in a phenol red-free medium containing 10 μM DCFDA. After incubation, the cells were washed again and irradiated with 200, 600, and 1000 mJ/cm^2 or kept in the dark as a control. For quantitative assessment, 125 μL of cell culture lysis reagent was added, and the cells were vortexed for 10 min. The cell lysates were measured at excitation/emission wavelengths of 485/520 nm for the green fluorescence of 2′7′-dichlorofluorescein (DCFH) using a microplate reader (FLUOStar Optima, BMG Labtech GmbH). The cells with "no treatment" and those treated with 50 μM *tert*-butyl hydroperoxide (TBHP) were used as negative and positive controls, respectively. The experiment was carried out in triplicate, and the mean fluorescence ± SD was considered. For qualitative assessment, after irradiation, the cells were washed and fixed using 4% paraformaldehyde, and the green fluorescence of DCFH was visualized. The cells were observed under a fluorescence microscope (CKX53 Olympus) with a B-excitation fluorescence mirror unit.

2.7. Statistical Analysis. All quantitative data are shown as the mean ± SD from at least three parallel groups. p values were determined by Student's t-test or two-way ANOVA (analysis of variance). Probability values of $p \leq 0.05$ (*), $p \leq 0.01$ (**), $p \leq 0.001$ (***), and $p \leq 0.0001$ (****) were considered statistically significant.

3. RESULTS AND DISCUSSION

3.1. Assessment of Liposome Formation. The co-encapsulation of a lower payload of a hydrophobic photosensitizer (hypericin) and nucleic acid (pDNA) was performed using a two-step approach (Scheme 1). The initial results showed an unimodal size distribution for empty liposomes (ELs). The dilution of ethanol with an aqueous buffer and ethanol evaporation favors the immediate formation of multilamellar liposomes.[31] The solvent ratio of ethanol to the aqueous medium during mixing was optimized to 25% (v/v). It was observed that the liposome size was dependent on the volumetric ratios of the two phases.[32,33] The average particle size and ζ-potential of DPPC:CH:DSPE-PEG2000 (84:15:1) ELs, determined by dynamic light scattering, were 115.5 ± 9.22 nm and −14.3 ± 2.60 mV, respectively. The polydispersity index (PDI = 0.19) confirmed that the prepared liposomes had the advantage of monomodal size distribution.[34] Because of PEG shielding, the slipping plane over ELs moved further away from the liposome surface, favoring a negative ζ-potential.[34]

https://doi.org/10.1021/acsami.4c10438
ACS Appl. Mater. Interfaces 2024, 16, 43416−43429

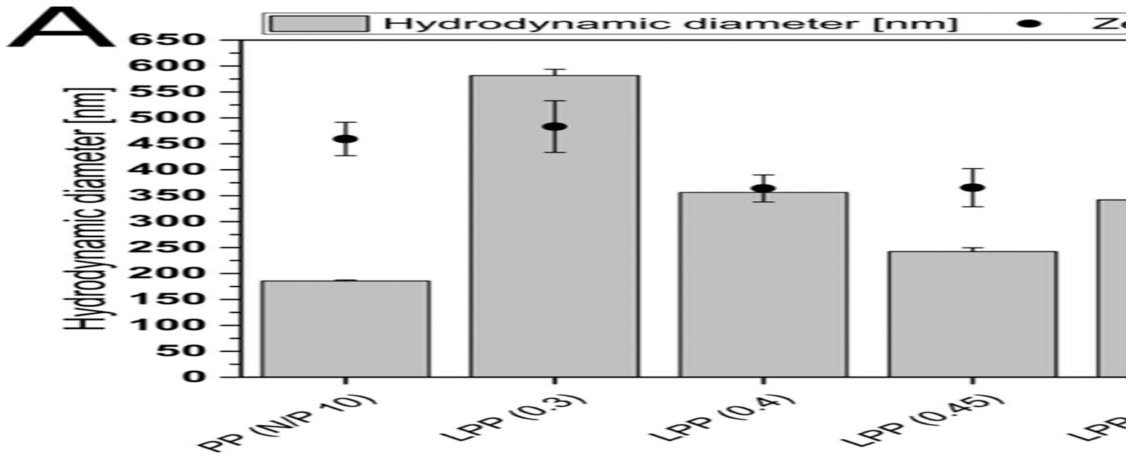

Figure 3. Average particle size and ζ-potential of (A) lipopolyplexes (LPP) prepared at a lipid:PEI mass ratio between 0.3 and 0.6 using empty liposomes and compared with polyplexes (PP) (N/P ratio = 10) and (B) hypericin lipopolyplexes (Hy-LPP) prepared using hypericin liposomes at a N/P ratio of 10 and lipid:PEI mass ratio of 0.45 and compared with LPP (0.45). Data are shown as mean ± SD (n = 3).

3.2. Physicochemical Characterization of Hypericin Formulations. HyLs were characterized using UV/vis spectroscopy, dynamic light scattering, and transmission electron microscopy. HyL prepared with tunable hypericin concentration under the given experimental conditions showed encapsulation efficiency of up to 80.2 ± 5.2% for 1 μM hypericin loading concentration. The UV/vis spectrum showed a bathochromic shift in the absorbance of HyL compared to that of 1 μM free hypericin in methanol (Figure 1A). Hypericin, incorporated into a thin phospholipid film (as described in Section 2), remains entrapped inside the lipid milieus during liposome formation because of its hydrophobicity.[16,35] Furthermore, the applied temperature was above the phase transition temperature of the lipid mixture, adding to the assumption that the hypericin molecules are incorporated deep inside the bilayer.[36] The encapsulation causes a shift in the absorbance of the cargo.[30,37] The effects of the hypericin loading concentration on the hydrodynamic diameter were investigated with hypericin concentrations ranging from 50 nM to 1 μM using dynamic light scattering (Table 1). Encapsulation of hypericin up to 500 nM increased the average particle diameter to 229.0 ± 8.20 nm. However, incorporating a higher hypericin concentration (1 μM) decreased the particle diameter to 198.5 ± 6.26 nm, which was still higher than the ELs' diameter. The negative surface charge on HyLs increased from −14.3 ± 2.60 mV to −31.2 ± 5.60 mV, which can be attributed to the encapsulation hypericin.[37] The polydispersity index of HyL was between 0.17 and 0.26, indicating a homogeneous monomodal distribution that underlines their stability.

Storage stability demonstrated a negligible change in the average size and ζ-potential (Figure 1B). Cholesterol mainly favored the structural stability and rigidity of the lipid bilayer, whereas the distal PEG tails on the surface of the formulation prevented particle aggregation.[24,38−40] These results were confirmed using a microscopic imaging technique. TEM images of the as-prepared EL and HyL (200 nM hypericin) exhibited homogeneous samples with spherical shapes and diameters of 100−20 nm and 160−190 nm, respecexperitively (Figure 1C,D).

3.3. Characterization of Hypericin Lipopolyplexes. Cationic polymer/pDNA complexes were examined using different approaches focusing on the binding affinity and complex integrity. It was observed that as the polymer concentration increased, free DNA migration was inhibited during gel electrophoresis (Figure 2A). In particular, for polyplexes lPEI/pDNA at an N/P ratio of 10, DNA migration was significantly reduced in an agarose bed, emphasizing the formation of complexes that entrap pDNA.[28] However, DLS analysis of lPEI/pDNA complexes showed broad size distributions (PDI ≥ 0.2) and might be related to incomplete condensation of DNA (Table S1).[40] Similarly, the fluorescence quenching assay showed 50% reduced fluorescence of SYBR intercalating dye with polyplexes at an N/P ratio 10 (Figure 2B).[19] Furthermore, the condensation efficiency of polyplexes with HyLs showed that Hy-LPP showed fluorescence quenching below 30% for all formulations containing >100 mM Hyp compared to free pDNA (Figure 2C). Based on these results, we can conclude that the hypericin concentration influenced fluorescence quenching at low lipid/PEI mass ratios, which was reduced by increasing the ratio. The reduced fluorescence suggested that Hy-LPP had a higher nucleic acid condensation ability than polyplexes, indicating that the HyLs shield the polyplexes.[18,41]

3.4. Physicochemical Characterization of Hypericin Lipopolyplexes. After pDNA encapsulation was confirmed, the particle sizes and ζ-potentials of the polyplexes and lipopolyplexes were determined using dynamic light scattering (Figure 3A). Polyplexes (N/P ratio = 10) and lipopolyplexes (N/P ratio = 10; lipid/PEI mass ratio = 0.45) showed minimum average particle sizes of 185.6 ± 7.74 nm and 242.1 ± 10.4 nm, respectively, and ζ-potentials of +11.2 ± 1.49 mV and +6.8 ± 5.70 mV, respectively. The densities of positive charges surrounding the polyplexes were reduced because of the complexation with the liposomes.[42,43] The results agreed with a study by Rezaee et al., who reported that lipopolyplex condensation of nucleic acids occurs at a lower C/P ratio (carrier/pDNA ratio) compared to that of the corresponding lipoplexes (lipid:pDNA complexes).[43] Hy-LPP possessed a mean hydrodynamic diameter between 230.2 ± 4.6 nm and 396.1 ± 6.9 nm and a slightly positive ζ-potential (Figure 3B). The incorporation of hypericin slightly increased the average particle size of Hy-LPP compared to LPP, although the change was independent of the hypericin concentration. HyL

https://doi.org/10.1021/acsami.4c10438
ACS Appl. Mater. Interfaces 2024, 16, 43416−43429

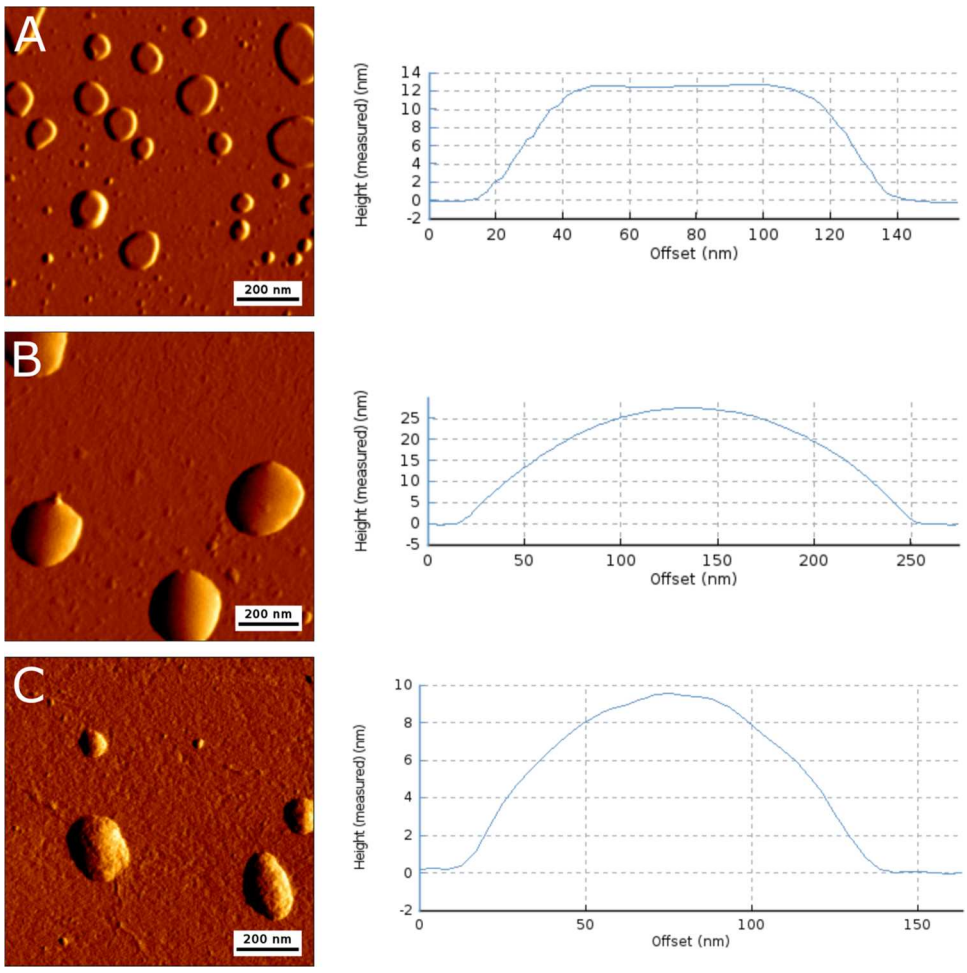

Figure 4. AFM micrographs to visualize the structure and surface morphology of DPPC:CH-DSPE:PEG2000 liposomes scanned in the amplitude mode at 1 μm × 1 μm (A) empty liposomes, (B) hypericin liposomes (200 nM hypericin), and (C) hypericin lipopolyplexes (50 nM hypericin and 0.5 μg of pDNA). Scale bars represent 200 nm. The height of the cross-sectional profile of respective formulations (right column).

formulations showed a reduced positive charge of polyplexes, confirming nucleic acid encapsulation.[42]

Atomic force microscopy was performed to examine the surface morphologies and particle diameters of EL, HyL, and Hy-LPP. These formulations were distinct, round, and well-shaped vesicles (Figure 4A–C). AFM diameters for EL, HyL, and Hy-LPP were 102.7 ± 2.98 nm, 214.8 ± 10.32 nm, and 226.8 ± 9.78 nm, respectively. The similarity between the hydrodynamic particle size and particle diameter measured by AFM confirmed the reproducibility of the method.

All in all, the physicochemical characterization of the formulations proved that Hy-LPP fulfilled the requisites that a gene carrier for intravenous administration of nucleic acids should have, e.g., the high encapsulation efficiency, small mean diameter, and overall positive surface charge.[40]

3.5. Cell Viability. *3.5.1. Evaluation of Hypericin Liposomes for Cell Viability.* Under dark conditions, the cells incubated with HyLs containing 50–500 nM hypericin showed maximum cell viability. It was observed that the cell viability remained at ∼80% for the nonirradiated cells. The results agreed with the hypericin's dark toxicity in Caco2 (IC_{50} = 2.5 μM), SW480 (IC_{50} = 5 μM), and HCT116 (IC_{50} = 2.5 μM).[37] Furthermore, HyL-treated cells were exposed to yellow light (λ_{587}) with increasing radiation exposures. A concentration-dependent decrease in cell viability was evident in the cells upon irradiation (Figure 5A). Cell viability was reduced in irradiated cells; however, a higher radiant exposure was necessary using 50 nM hypericin compared to 500 nM hypericin. Cells treated with EL were considered as controls. HyLs incubated in nonirradiated cells were observed to be nontoxic until they reached their effective dose of IC_{50} = 2.5 μM (Table S2). The results also emphasize a considerable reduction in cell viability at radiant exposures of 200 mJ/cm^2 (p < 0.01) and 1000 mJ/cm^2 (p < 0.001). As irradiation fluency increases, the effective dose of hypericin-induced cytotoxicity (IC_{50} values) reduces exponentially.[44] At 600 mJ/cm^2, a significantly reduced hypericin dose (IC_{50} = 202 nM) was reported. Moreover, the cells treated with HyL (200 nM hypericin) exhibited cell viabilities of around 80% (for values ≤400 mJ/cm^2) and 50% (for values ≥600 mJ/cm^2) with lower and higher radiant exposures, respectively. The results suggested that the degree of cytotoxicity of hypericin in HepG2 cells might be associated with the extent of intracellular photochemical reactions.[45] It was reported from our group that hypericin liposome formulations showed cytotoxic effects at IC_{50} 237 nM with SKOV-3 cells at 2.1 J/cm^2 and IC_{50} 90.8 nM with MDA-MB-231 cells at 1.6 J/cm^2.[16,30] An effective IC_{50} value of hypericin depends on the cellular internalization of hypericin, which is solely determined by the physicochemical

https://doi.org/10.1021/acsami.4c10438
ACS Appl. Mater. Interfaces 2024, 16, 43416–43429

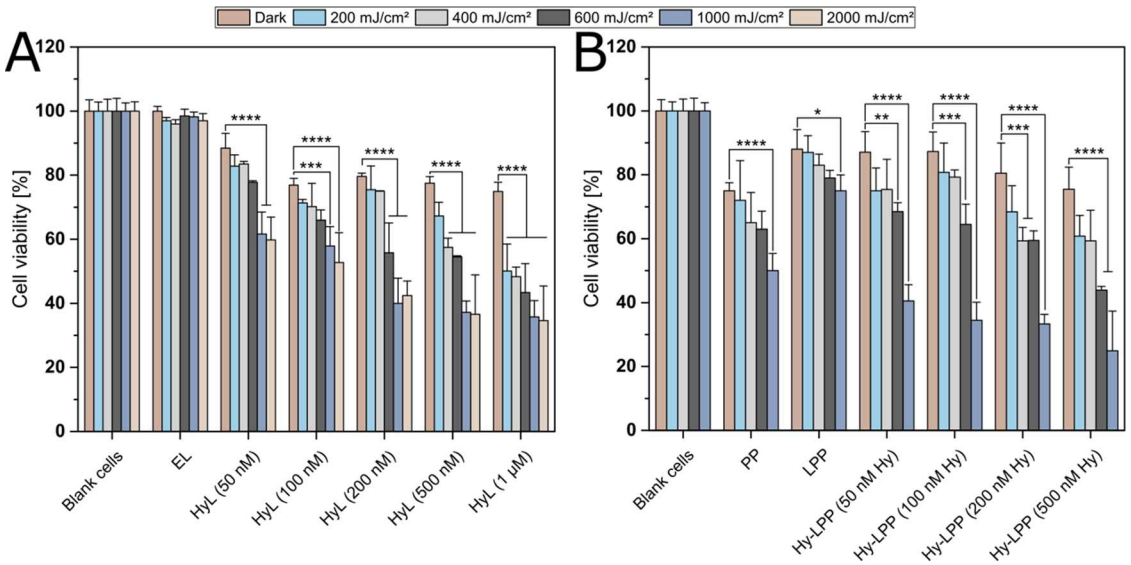

Figure 5. Cell viability of HepG2 cells incubated with hypericin formulations followed by irradiation with different radiant exposures. (A) % Cell viability of cells treated with empty liposomes (EL) and hypericin liposomes (HyL) (50 nM to 1 μM hypericin); (B) cell viability of cells treated with polyplex (PP), lipopolyplex (LPP), and hypericin lipopolyplexes (Hy-LPP) prepared at a lipid:PEI mass ratio of 0.45 using HyLs (50−500 nM hypericin). Cells treated with 0.1% Triton-X100 were considered positive controls, and untreated cells were considered as controls. The cells kept under dark conditions were considered negative controls for the respective formulation. Data are shown as mean ± SD (n = 3). Probability values of $p \leq 0.05$ (*), $p \leq 0.01$ (**), $p \leq 0.001$ (***), and $p \leq 0.0001$ (****) were considered statistically significant.

characteristics of the hypericin formulation and the type of cell line.[37]

These results suggest that it is possible to apply a lower radiant exposure to significantly reduce cell viability if a higher hypericin concentration is used. However, increasing the radiant exposure and hypericin concentration did not improve this effect.

3.5.2. Evaluation of Hypericin Lipopolyplexes for Cell Viability. The multicomponent hypericin lipopolyplexes containing different hypericin concentrations (50−500 nM hypericin) and a constant concentration of pDNA were evaluated in nonirradiated and irradiated cells (Figure 5B). Under dark conditions, the viability of cells treated with polyplexes was reduced to 75.0 ± 2.5%, while LPP showed higher cell viability. It was evident that the internalization of polyplexes led to PEI-mediated cytotoxicity.[46] The cell damage caused by polyplexes was reduced by LPP and Hy-LPP formulations.[18,19] In comparison with nonirradiated cells, the cells exposed to 600 mJ/cm^2 exhibited negligible reduction, while the strongest reduction in cell viability was observed at 1000 mJ/cm^2. The cell death observed with hypericin treatment and irradiation at a higher radiant exposure was interpreted as a hypericin-induced photodynamic effect. Further, evaluation of the right balance between radiant exposure and hypericin concentration is essential since, in the end, this balance enhances the carrier's transfection efficiency. The cells incubated with Hy-LPP (≤100 nM hypericin) and irradiated with a radiant exposure of ≤600 mJ/cm^2 did not exhibit retarded cell viability. Cell death was observed using a higher photochemical dose (radiant exposure and hypericin concentration). This interpretation harmonized with findings that the light energy required to induce PCI is much lower than that required to induce PDT in cancer cells.[47] Hence, 200, 600, and 1000 mJ/cm^2 were selected for evaluating phototransfection using hypericin lipopolyplexes (50−500 nM hypericin) in HepG2 cells.

3.6. In Vitro Transfection Experiments. The proof-of-concept for improved transfection using the PCI technique is based on the simultaneous intracellular delivery of macromolecules and photosensitizers incorporated into one nanocarrier. The irradiation was performed with a standard "light after" protocol at a 2 h post-transfection interval. It has been reported elsewhere that the relative effect of light treatment decreases with longer post-transfection incubation time (4 h) in the "light after" protocol.[48]

3.6.1. Phototransfection. Cells were incubated with hypericin lipopolyplexes (50−500 nM hypericin) followed by post-transfection irradiation at 200, 600, and 1000 mJ/cm^2 fluence rates. Cells transfected with free pDNA, polyplexes, and lipopolyplexes in the dark were considered as controls (Figure 6A). It was observed that PCI significantly improved the transfection efficiency of lPEI/pDNA complexes when irradiation was applied at 600 mJ/cm^2. lPEI demonstrates the "proton sponge effect" because the pK values of its amino group are close to the intracellular endosomal pH. Upon exposure to light, this synergistic effect is attributed to PCI accelerating "the buffering capacity" of the lPEI. lPEI protects nucleic acids from in vitro photodegradation. SYBR quenching and gel electrophoresis assay results supported the assumption that lPEI protects the nucleic acid from in vitro photodegradation.[38,49] It was reported elsewhere that the PCI effect on the lipid-based nonviral carrier depends on the formulation's structure for the transfection regimen.[48]

Further, 0.25 μg of pCMV-Luc was codelivered with 50−500 nM hypericin using Hy-LPP, and the transfection efficiency was compared with that of lipopolyplexes. When the transfected cells were exposed to 200 mJ/cm^2, transfection was hindered only for the formulation with 500 nM hypericin. A substantial increase in transfection efficiency has been reported for cells irradiated at a concentration of 600 mJ/cm^2. These results suggest a photoselective transfection induced by a photochemical reaction initiated by the excitation of the delivered photosensitizer. The photoselective transfection of

https://doi.org/10.1021/acsami.4c10438
ACS Appl. Mater. Interfaces 2024, 16, 43416−43429

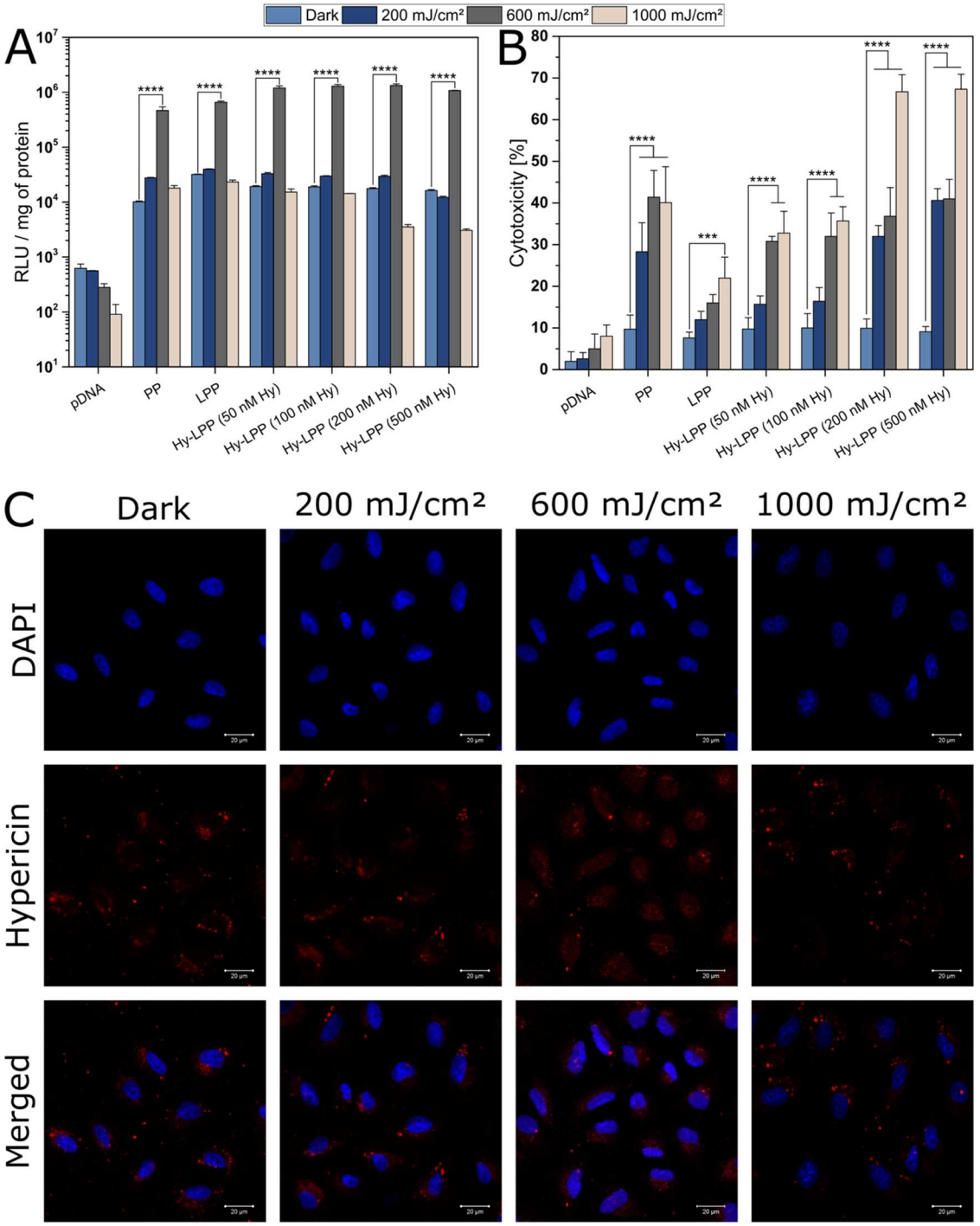

Figure 6. (A) Bright-glow luciferase assay to determine transfection efficiency. Hypericin lipopolyplexes were transfected and exposed to irradiation at 200, 600, and 1000 mJ/cm^2 using an LED with wavelength λ_{587}. The cells kept in the dark were used as positive controls for the respective formulation. Data are shown as mean ± SD (n = 3). Probability values of $p \leq 0.0001$ (****) are considered statistically significant. (B) Cytotoxicity determined by LDH assay. Hypericin lipopolyplexes were transfected and exposed to irradiation at 200, 600, and 1000 mJ/cm^2 using an LED with wavelength λ_{587}. The assays were multiplexed using a cytotoxicity assay upstream of the luciferase assay. The cells kept in the dark were used as positive controls for the respective formulations. Data are shown as mean ± SD (n = 3). Probability values of $p \leq 0.001$ (***) and $p \leq 0.0001$ (****) are considered statistically significant. (C) Cellular distribution of hypericin lipopolyplexes encapsulating 1 μg of pDNA and 50 nM hypericin. The cells were incubated with the formulation for 2 h at 37 °C and irradiated with different radiant exposures: 200, 600, and 1000 mJ/cm^2. Each formulation contained 1 μg of pDNA and 50 nM hypericin. DAPI-stained nuclei are colored blue, and hypericin in the cytoplasm is colored red. Scale bars are 20 μm.

Hy-LPP (600 mJ/cm^2) increased 60- to 75-fold compared with that in nonirradiated cells. Additionally, the transfection enhancement in the irradiated cells by Hy-LPP was approximately 2-fold higher than that by LPP. Irradiation at 1000 mJ/cm^2 decreased the transfection efficiency below the respective value of the dark control. These results suggest that there could be multiple reasons for the low transfection efficiency of nonirradiated cells. However, the most likely

https://doi.org/10.1021/acsami.4c10438
ACS Appl. Mater. Interfaces 2024, 16, 43416−43429

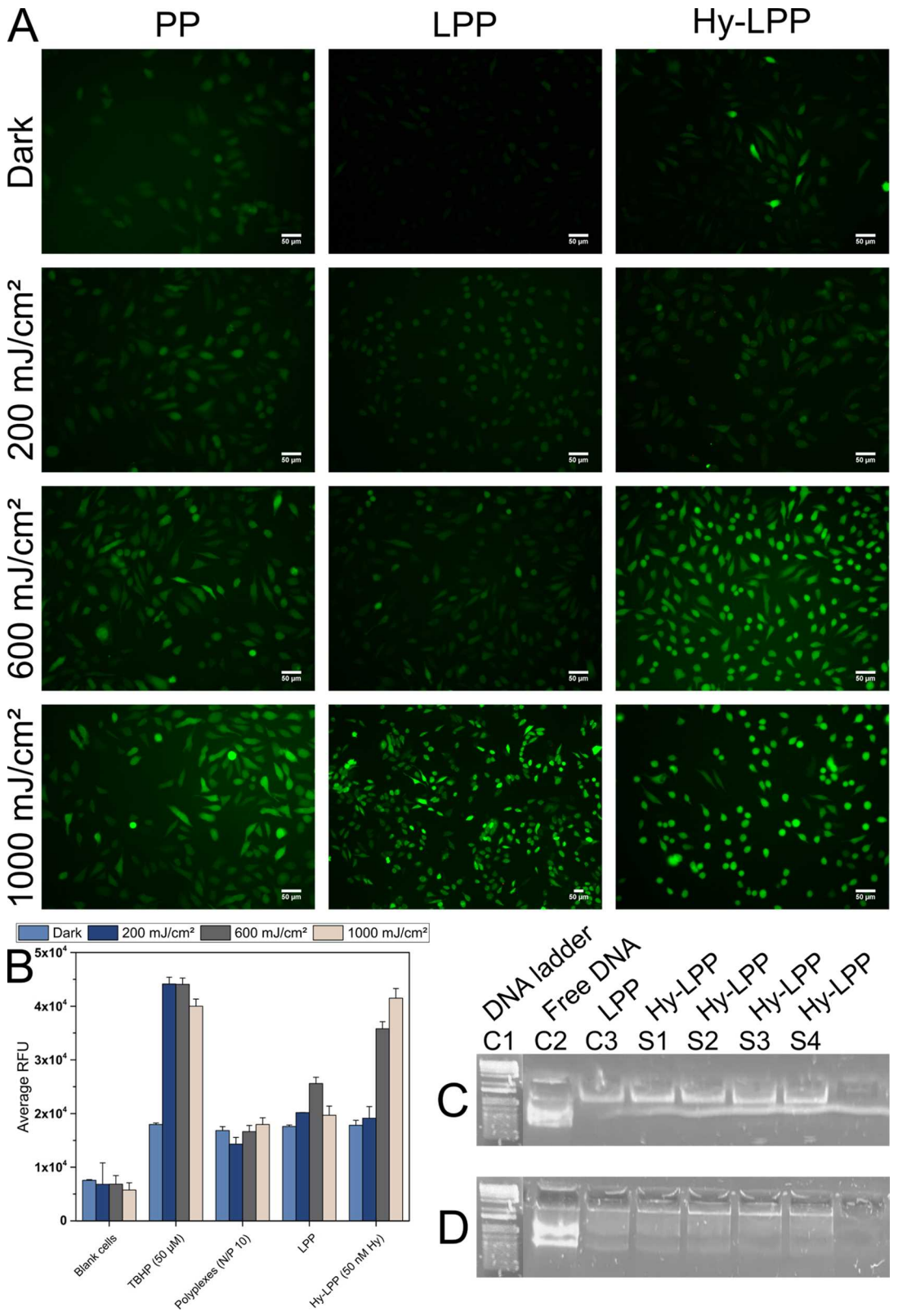

Figure 7. (A) Visualization of the green fluorescence of DCFH using an Olympus microscope. Scale bars represent 50 μm. (B) Reactive oxygen spices (ROS) generation in HepG2 cells transfected with polyplexes, lipopolyplexes, and hypericin lipopolyplexes (50 nM hypericin) and irradiated at different radiant exposures (200, 600, and 1000 mJ/cm^2) quantified by measuring DCFH using a FLUOstar Optima multiplate reader. Cells treated with TBHP (50 μM) were considered as positive control, and cells without treatment were considered as negative control. Data are shown as mean ± SD (n = 3). (C, D) Photostability of pDNA in hypericin lipopolyplexes (50−500 nM hypericin) after irradiation. The samples contain 0.25 μg pDNA in each sample and 50 nM (S1), 100 nM (S2), 200 nM (S3), and 500 nM (S4) hypericin. Each formulation was irradiated at 600 mJ/cm^2 using an LED with a wavelength λ_{587} followed by electrophoresis. (C) Irradiated and nonlysed formulations and (D) irradiated and lysed formulations. The results are compared with those obtained using free DNA and a DNA ladder as controls.

https://doi.org/10.1021/acsami.4c10438
ACS Appl. Mater. Interfaces 2024, 16, 43416−43429

reason could be poor internalization because of the steric hindrance by the PEG chain on the surface of the carrier or poor endosomal escape.[38] The results strongly suggest that the reduced transfection efficiency exhibited in irradiated cells by the respective formulations was due to an excessive photochemical dose. This effect can be attributed to increased photocytotoxicity.[24] Conversely, the elevated transfection upon irradiation at 600 mJ/cm^2 (an optimal radiant exposure) resulted in an adequate photochemical dose that induces a photochemical reaction without significantly compromising cell viability.[1,50] The photochemical reaction leads to cell membrane disruption because of lipid peroxidation by $^1O_2$ generation, while PS without irradiation does not induce any membrane disruption.[29,51]

3.6.2. Photocytotoxicity. The cytotoxicity of cells transfected with PP, LPP, and Hy-LPP was assessed and is displayed in Figure 6B. The nonirradiated cells incubated with Hy-LPP containing 50−500 nM hypericin demonstrated negligible cytotoxicity, indicating suitable biocompatibility of the formulation, which is essential for its application as a gene delivery system. At 600 mJ/cm^2, cytotoxicity increased to 30% for Hy-LPP (Hy ≤ 100 nM). However, irradiation of treated cells at 1000 mJ/cm^2 significantly boosted the cytotoxic effect ($p < 0.0001$). Relocalization of the photosensitizer during light exposure has previously been described for other amphiphilic photosensitizers, and their second location sites have been proposed to play an important role in cytotoxicity.[17,52] It was reported that >100 nM hypericin showed 70% cytotoxicity to HepG2 cells at 1000 mJ/cm^2. These results were attributed to the photodynamic activity of hypericin at the applied photochemical dose. A synergistic antitumor therapy can be proposed for hypericin lipopolyplexes containing siRNA as a therapeutic gene. The hypericin-induced photodynamic effect and efficient knockdown of the gene of interest upon photoselective transfection in the remaining viable cells were predicted.

Finding the appropriate parameters with these complex formulations to maximize phototransfection and minimize photocytotoxicity is even more difficult in in vivo studies. Nevertheless, recent research has demonstrated the potential and selectivity of PCI. Suzuki et al. prepared polymer−lipid nanoparticles (PLNs) and effectively encapsulated TPPS2a and TNFα siRNA. They demonstrated increased cytokine silencing after irradiation because of PCI-mediated endosomal/lysosomal escape, preventing psoriatic plaque formation in hairless mice.[53] Zhang et al. codelivered a photoactivatable Pt(IV) prodrug and siRNA. After irradiation of the xenograft mice model, the prodrug was activated, and an endosomal/lysosomal escape was induced, leading to successful downregulation and reduced tumor weight.[54]

3.7. Intracellular Effect of Irradiation. For the implementation of photochemical internalization, the formulation should meet three essential requirements in addition to a small diameter and biocompatibility: (i) cellular internalization of the formulation,[15] (ii) photochemical reaction in the cells upon irradiation at suboptimal radiant exposure,[12] and (iii) photostability of the delivered gene upon irradiation of the photosensitizer with a suboptimal radiant exposure.[27]

3.7.1. Cellular Uptake and Distribution. The seeded HepG2 cells were treated with free hypericin (free Hy) dissolved in DMSO, HyLs, and Hy-LPPs for 1, 2, 4, 6, and 24 h, and cellular uptake was evaluated by counterstaining with DAPI and Phalloidin 488 (F-actin staining) and capturing CLSM images (see Section 1.1 in the Supporting Information). Whereas free Hy accumulated in the cell membrane of the cells and its fluorescence covered an area similar to that of F-actin staining after all incubation times, the fluorescence of HyLs and Hy-LPPs was restricted to smaller spots inside the cells, hinting at endosomal/lysosomal uptake (see Figures S1−S5 in the Supporting Information). The uptake or the amount and intensity of the spots increased during incubation; however, these high concentrations and incubation times led to significant cytotoxicity when irradiated. Thus, lower concentrations and limited incubation times are required to assess the endosomal/lysosomal escape and cellular distribution.

The cells were incubated with Hy-LPP (50 nM hypericin) for 2 h, followed by irradiation at 200, 600, and 1000 mJ/cm^2 or under dark conditions. The red fluorescence of internalized hypericin was promptly analyzed by confocal laser scanning microscopy (Figure 6C). The nonirradiated cells exhibited clump-like fluorescence areas and insufficient intracellular distribution, suggesting insufficient ROS generation. Similar results were obtained after irradiation at 200 and 1000 mJ/cm^2, with the latter possibly causing excess ROS generation leading to high phototoxicity. Using only 600 mJ/cm^2 resulted in a distinct red fluorescence throughout the cytoplasm. The change in the distribution of Hy-LPP was attributed to an improved endosomal/lysosomal escape.[10,52] It seems that the photochemical reaction was sufficient enough to disrupt the endosomal/lysosomal membrane.[55,56]

3.7.2. Intracellular Reactive Oxygen Species. Intracellular reactive oxygen species (ROS) were measured using DCFH-DA staining. The resultant intracellular DCFH emits detectable green fluorescence proportional to the amount of ROS produced by photochemical reactions with hypericin. ROS generation was quantified using a microplate reader (Figure 7B). The relative fluorescence units measured in the different cells showed a pattern: nonirradiated cells incubated with PP and LPP < nonirradiated cells incubated with Hy-LPP < irradiated cells incubated with Hy-LPP < TBHP treated cells. It was observed that Hy-LPP showed significantly higher fluorescence intensity (3-fold increase) at 600 and 1000 mJ/cm^2 compared to nonirradiated cells. Photoexcitation of internalized hypericin (50 nM) induced intracellular ROS generation.[30,44] Further, visualization of the cells treated with a similar treatment proved that the results were consistent with the quantitative results (Figure 7A). For Hy-LPP, the fluorescence in cells irradiated at 1000 mJ/cm^2 was more potent than that in cells irradiated with a lower radiant exposure. ROS production was dependent on the intensity of the exposed photochemical dose.[45,57] Interestingly, both evaluations showed ROS generation in cells treated with polyplexes and lipopolyplexes at higher radiant exposure, presumably caused by an augmented intracellular concentration of polycationic lPEI.[58] The elevated ROS production at 1000 mJ/cm^2 showed a round cellular structure, which could be attributed to the cytotoxic effect of hypericin. Cytotoxicity and ROS quantification confirmed that excess hypericin might photochemically damage organelles such as mitochondria or endoplasmic reticulum after endosomal/lysosomal escape.[10,45] It was rationalized that 600 mJ/cm^2 (a suitable suboptimal radiant exposure) does not cause cell death but facilitates cellular distribution and transfection efficiency because of minimum ROS generation. The results are promising and support the idea of site-specific gene delivery using irradiation.[59,60]

https://doi.org/10.1021/acsami.4c10438
ACS Appl. Mater. Interfaces 2024, 16, 43416−43429

3.8. Photostability of Genes in Hypericin Lipopolyplexes. A nonviral carrier must have the crucial characteristic of segregating the photosensitizer and genetic material. Hence, assessing the photodegradation of the delivered nucleic acids by agarose gel electrophoresis is important. Hy-LPP formulations containing 50, 100, 200, and 500 nM hypericin were irradiated at 600 mJ/cm^2 and electrophoresed. No DNA bands were observed on the agarose bed (Figure 7C). In contrast, DNA migration was observed when the Hy-LPP formulations were lysed after irradiation (Figure 7D). It was interpreted that lPEI protects the nucleic acids.[29,61] Thus, partitioning of the nucleic acid and photosensitizer inside the formulation was proven. The low radiant exposure, as mentioned above, has no safety-relevant issues and thus has a clinical significance.[56]

4. CONCLUSIONS

The instability, low payload, and inefficient transfection of standard DNA delivery systems limit their application in gene therapy. Hypericin lipopolyplexes are promising, efficient nonviral gene carriers that can overcome these barriers. The formulation consisted of a core compartment encapsulating therapeutic pDNA that protected it from enzymatic degradation. Successful encapsulation of hypericin into the phospholipid layer of the liposome formulation eliminates its negative interactions with the biological compartment and the photocytotoxicity of the free photosensitizer. The hypericin lipopolyplexes exhibited reduced size, positive surface charge, and higher encapsulation efficiency for nucleic acids and photosensitizer, demonstrating the photostability of the delivered genetic material. Upon irradiation at 600 mJ/cm^2, hypericin at concentrations ≤200 nM effectively increased the luciferase expression in HepG2 cells. The results emphasize that combining the photosensitizer concentration and radiant exposure determines the balance between transfection efficiency and cytotoxicity. Enhanced transfection was attributed to increased intracellular ROS generation and endosomal/lysosomal escape. Thus, lipopolyplexes are valuable for application as light-sensitive gene delivery systems. Therefore, the synergistic effect of the developed nanocarrier holds potential for anticancer gene therapy of hepatocellular carcinoma. Further experiments in xenograft models will elucidate the selectivity and capability of this "light after" strategy.

■ ASSOCIATED CONTENT

Supporting Information

The Supporting Information is available free of charge at https://pubs.acs.org/doi/10.1021/acsami.4c10438.

Additional experimental data including particle size (hydrodynamic diameter), polydispersity index, and ζ-potential of polyplexes (lPEI/pDNA) measured using a Zetasizer Nano ZS (Malvern Panalytical GmbH, Kassel, Germany) (Table S1), IC_{50} values of hypericin liposomes at different radiant exposures (27 W/cm^2 and 587 nm) using a prototype low-power light-emitting diode (Lumundus, Eisenach, Germany) against HepG2 cells (Table S2), and cellular uptake of free hypericin (free Hy) dissolved in DMSO, hypericin liposomes (HyLs), and hypericin lipopolyplexes (Hy-LPPs) after 1, 2, 4, 6, and 24 h of incubation (Figures S1−S5) (PDF)

■ AUTHOR INFORMATION

Corresponding Authors

Eduard Preis − *Department of Pharmaceutics and Biopharmaceutics, University of Marburg, 35037 Marburg, Germany;* orcid.org/0000-0003-2112-8436; Email: eduard.preis@pharmazie.uni-marburg.de

Udo Bakowsky − *Department of Pharmaceutics and Biopharmaceutics, University of Marburg, 35037 Marburg, Germany;* orcid.org/0000-0002-3895-0453; Email: ubakowsky@aol.com

Authors

Hirva Shah − *Department of Pharmaceutics and Biopharmaceutics, University of Marburg, 35037 Marburg, Germany*

Sebastian Schlüter − *Department of Pharmaceutics and Biopharmaceutics, University of Marburg, 35037 Marburg, Germany*

Muhammad Umair Amin − *Department of Pharmaceutics and Biopharmaceutics, University of Marburg, 35037 Marburg, Germany*

Alice Abu Dayyih − *Department of Pharmaceutics and Biopharmaceutics, University of Marburg, 35037 Marburg, Germany*

Konrad H. Engelhardt − *Department of Pharmaceutics and Biopharmaceutics, University of Marburg, 35037 Marburg, Germany*

Shashank Reddy Pinnapireddy − *Department of Pharmaceutics and Biopharmaceutics, University of Marburg, 35037 Marburg, Germany;* Present Address: CSL Behring GmbH, Emil-von-Behring-Str. 76, Marburg 35041, Germany; orcid.org/0000-0003-4036-7619

Complete contact information is available at: https://pubs.acs.org/10.1021/acsami.4c10438

Author Contributions

‡H.S., S.S., and M.U.A. contributed equally to this work. H.S. contributed to the conceptualization, methodology, investigation, and writing of the manuscript. S.S. and M.U.A. contributed to the conceptualization, methodology, investigation, and writing−review and editing. A.A.D. and K.H.E. contributed to the investigation. S.R.P. contributed to the visualization, writing−review, and editing of the manuscript. E.P. and U.B. contributed to the conceptualization, supervision, visualization, writing−review, and editing of the manuscript.

Notes

The authors declare no competing financial interest.

■ ACKNOWLEDGMENTS

The authors would like to thank Mrs. Eva Mohr for her technical support in the cell culture laboratory. Parts of the images were drawn by using pictures from Servier Medical Art. Servier Medical Art by Servier is licensed under a Creative Commons Attribution 3.0 Unported License.

■ ABBREVIATIONS

DPPC1,2-dipalmitoyl-*sn*-glycero-3-phosphocholine; DSPE-PEG1,2-distearoyl-*sn*-glycero-3-phosphoethanolamine-*N*-[methoxy (polyethylene glycol); CHcholesterol; Hy-LPPhypericin lipopolyplexes; LDHlactate dehydrogenase; ROSreactive oxygen species; ODNoligonucleotides; PNApeptide nucleic acids;

https://doi.org/10.1021/acsami.4c10438
ACS Appl. Mater. Interfaces 2024, 16, 43416−43429

PCIphotochemical internalization; PSphotosensitizer; lPEI-linear polyethylenimine; PEGpolyethylene glycol; RESreticuloendothelial system; EEencapsulation efficiency; AFMatomic force microscopy; TBHP*tert*-butyl hydroperoxide; PDIpolydispersity index; ELempty liposome; HyLhypericin liposome; PPpolyplexes; DLSdynamic light scattering; PDTphotodynamic therapy

REFERENCES

(1) Berg, K.; Folini, M.; Prasmickaite, L.; Selbo, P.; Bonsted, A.; Engesaeter, B.; Zaffaroni, N.; Weyergang, A.; Dietzea, A.; Maelandsmo, G.; Wagner, E.; Norum, O.-J.; Hogset, A. Photochemical Internalization: A New Tool for Drug Delivery. *Curr. Pharm. Biotechnol.* **2007**, *8* (6), 362−372.

(2) Jerjes, W.; Theodossiou, T. A.; Hirschberg, H.; Høgset, A.; Weyergang, A.; Selbo, P. K.; Hamdoon, Z.; Hopper, C.; Berg, K. Photochemical Internalization for Intracellular Drug Delivery. From Basic Mechanisms to Clinical Research. *J. Clin. Med.* **2020**, *9* (2), No. 528, DOI: 10.3390/jcm9020528.

(3) Ewe, A.; Panchal, O.; Pinnapireddy, S. R.; Bakowsky, U.; Przybylski, S.; Temme, A.; Aigner, A. Liposome-polyethylenimine complexes (DPPC-PEI lipopolyplexes) for therapeutic siRNA delivery in vivo. *Nanomedicine* **2017**, *13* (1), 209−218, DOI: 10.1016/j.nano.2016.08.005.

(4) Oster, C. G.; Wittmar, M.; Bakowsky, U.; Kissel, T. DNA nanocarriers from biodegradable cationic branched polyesters are formed by a modified solvent displacement method. *J. Controlled Release* **2006**, *111* (3), 371−381, DOI: 10.1016/j.jconrel.2005.12.004.

(5) Shahryari, A.; Burtscher, I.; Nazari, Z.; Lickert, H. Engineering Gene Therapy: Advances and Barriers. *Adv. Ther.* **2021**, *4* (9), No. 2100040.

(6) Nishiyama, N.; Iriyama, A.; Jang, W.-D.; Miyata, K.; Itaka, K.; Inoue, Y.; Takahashi, H.; Yanagi, Y.; Tamaki, Y.; Koyama, H.; Kataoka, K. Light-induced gene transfer from packaged DNA enveloped in a dendrimeric photosensitizer. *Nat. Mater.* **2005**, *4* (12), 934−941.

(7) Berg, K.; Selbo, P. K.; Prasmickaite, L.; Tjelle, T. E.; Sandvig, K.; Moan, J.; Gaudernack, G.; Fodstad, O.; Kjølsrud, S.; Anholt, H.; Rodal, G. H.; Rodal, S. K.; Høgset, A. Photochemical internalization: a novel technology for delivery of macromolecules into cytosol. *Cancer Res.* **1999**, *59* (6), 1180−1183.

(8) Soe, T. H.; Watanabe, K.; Ohtsuki, T. Photoinduced Endosomal Escape Mechanism: A View from Photochemical Internalization Mediated by CPP-Photosensitizer Conjugates. *Molecules* **2021**, *26* (1), No. 36, DOI: 10.3390/molecules26010036.

(9) Høgset, A.; Prasmickaite, L.; Selbo, P. K.; Hellum, M.; Engesaeter, B. Ø.; Bonsted, A.; Berg, K. Photochemical internalisation in drug and gene delivery. *Adv. Drug Delivery Rev.* **2004**, *56* (1), 95−115.

(10) Jayakumar, M. K. G.; Bansal, A.; Huang, K.; Yao, R.; Li, B. N.; Zhang, Y. Near-Infrared-Light-Based Nano-Platform Boosts Endosomal Escape and Controls Gene Knockdown in Vivo. *ACS Nano* **2014**, *8* (5), 4848−4858.

(11) Oliveira, S.; Hogset, A.; Storm, G. Delivery of siRNA to the Target Cell Cytoplasm: Photochemical Internalization Facilitates Endosomal Escape and Improves Silencing Efficiency, In Vitro and In Vivo. *Curr. Pharm. Des.* **2008**, *14* (34), 3686−3697.

(12) Selbo, P. K.; Kristian, l.; Høgset, A.; Prasmickaite, L.; Berg, K. Photochemical Internalisation: A Novel Drug Delivery System. *Tumor Biol.* **2002**, *23* (2), 103−112.

(13) Dechêne, A.; Kasper, S.; Olivecrona, H.; Schirra, J.; Trojan, J. Photochemical internalization and gemcitabine combined with first-line chemotherapy in perihilar cholangiocarcinoma: observations in three patients. *Endosc. Int. Open* **2020**, *08* (12), E1878−E1883, DOI: 10.1055/a-1276-6366.

(14) Berg, K.; Nordstrand, S.; Selbo, P. K.; Tran, D. T. T.; Angell-Petersen, E.; Høgset, A. Disulfonated tetraphenyl chlorin (TPCS2a), a novel photosensitizer developed for clinical utilization of photochemical internalization. *Photochem. Photobiol. Sci.* **2011**, *10* (10), 1637−1651, DOI: 10.1039/c1pp05128h.

(15) Berlanda, J.; Kiesslich, T.; Engelhardt, V.; Krammer, B.; Plaetzer, K. Comparative in vitro study on the characteristics of different photosensitizers employed in PDT. *J. Photochem. Photobiol., B* **2010**, *100* (3), 173−180.

(16) Plenagl, N.; Duse, L.; Seitz, B. S.; Goergen, N.; Pinnapireddy, S. R.; Jedelska, J.; Brüßler, J.; Bakowsky, U. Photodynamic therapy − hypericin tetraether liposome conjugates and their antitumor and antiangiogenic activity. *Drug Delivery* **2019**, *26* (1), 23−33.

(17) Agostinis, P.; Vantieghem, A.; Merlevede, W.; de Witte, P. A. M. Hypericin in cancer treatment: more light on the way. *Int. J. Biochem. Cell Biol.* **2002**, *34* (3), 221−241, DOI: 10.1016/s1357-2725(01)00126-1.

(18) Otterhaug, T.; Janetzki, S.; Welters, M. J. P.; Håkerud, M.; Nedberg, A. G.; Edwards, V. T.; Boekestijn, S.; Loof, N. M.; Selbo, P. K.; Olivecrona, H.; van der Burg, S. H.; Høgset, A. Photochemical Internalization Enhanced Vaccination Is Safe, and Gives Promising Cellular Immune Responses to an HPV Peptide-Based Vaccine in a Phase I Clinical Study in Healthy Volunteers. *Front. Immunol.* **2021**, *11*, No. 576756.

(19) Shah, H.; Tariq, I.; Engelhardt, K.; Bakowsky, U.; Pinnapireddy, S. R. Development and Characterization of Ultrasound Activated Lipopolyplexes for Enhanced Transfection by Low Frequency Ultrasound in In Vitro Tumor Model. *Macromol. Biosci.* **2020**, *20* (12), No. 2000173.

(20) Pinnapireddy, S. R.; Duse, L.; Strehlow, B.; Schäfer, J.; Bakowsky, U. Composite liposome-PEI/nucleic acid lipopolyplexes for safe and efficient gene delivery and gene knockdown. *Colloids Surf., B* **2017**, *158*, 93−101.

(21) Younis, M. A.; Khalil, I. A.; Harashima, H. Gene Therapy for Hepatocellular Carcinoma: Highlighting the Journey from Theory to Clinical Applications. *Adv. Ther.* **2020**, *3* (11), No. 2000087.

(22) Lind, P. A.; Naucler, G.; Holm, A.; Gubanski, M.; Svensson, C. Efficacy of pegylated liposomal doxorubicin in patients with advanced hepatocellular carcinoma. *Acta Oncol.* **2007**, *46* (2), 230−233.

(23) Pinnapireddy, S. R.; Duse, L.; Akbari, D.; Bakowsky, U. Photo-Enhanced Delivery of Genetic Material Using Curcumin Loaded Composite Nanocarriers. *Clin. Oncol.* **2017**, *2*, No. 1323, DOI: 10.25107/2474-1663.1323.

(24) Selbo, P. K.; Weyergang, A.; Høgset, A.; Norum, O.-J.; Berstad, M. B.; Vikdal, M.; Berg, K. Photochemical internalization provides time- and space-controlled endolysosomal escape of therapeutic molecules. *J. Controlled Release* **2010**, *148* (1), 2−12, DOI: 10.1016/j.jconrel.2010.06.008.

(25) Brüßler, J.; Marxer, E.; Becker, A.; Schubert, R.; Schümmelfeder, J.; Nimsky, C.; Bakowsky, U. Correlation of structure and echogenicity of nanoscaled ultrasound contrast agents in vitro. *Colloids Surf., B* **2014**, *117*, 206−215.

(26) Engelhardt, K. H.; Pinnapireddy, S. R.; Baghdan, E.; Jedelská, J.; Bakowsky, U. Transfection Studies with Colloidal Systems Containing Highly Purified Bipolar Tetraether Lipids from Sulfolobus acidocaldarius. *Archaea* **2017**, *2017*, 1−12.

(27) Amin, M. U.; Ali, S.; Tariq, I.; Ali, M. Y.; Pinnapreddy, S. R.; Preis, E.; Wölk, C.; Harvey, R. D.; Hause, G.; Brüßler, J.; Bakowsky, U. Ultrasound-Responsive Smart Drug Delivery System of Lipid Coated Mesoporous Silica Nanoparticles. *Pharmaceutics* **2021**, *13* (9), No. 1396, DOI: 10.3390/pharmaceutics13091396.

(28) Raval, N.; Jogi, H.; Gondaliya, P.; Kalia, K.; Tekade, R. K. Method and its Composition for encapsulation, stabilization, and delivery of siRNA in Anionic polymeric nanoplex: An In vitro- In vivo Assessment. *Sci. Rep.* **2019**, *9* (1), No. 16047, DOI: 10.1038/s41598-019-52390-4.

(29) Nomoto, T.; Fukushima, S.; Kumagai, M.; Machitani, K.; Arnida; Matsumoto, Y.; Oba, M.; Miyata, K.; Osada, K.; Nishiyama, N.; Kataoka, K. Three-layered polyplex micelle as a multifunctional nanocarrier platform for light-induced systemic gene transfer. *Nat. Commun.* **2014**, *5* (1), No. 3545, DOI: 10.1038/ncomms4545.

(30) Dayyih, A. A.; Alawak, M.; Ayoub, A. M.; Amin, M. U.; Dayyih, W. A.; Engelhardt, K.; Duse, L.; Preis, E.; Brüßler, J.; Bakowsky, U. Thermosensitive liposomes encapsulating hypericin: Characterization and photodynamic efficiency. *Int. J. Pharm.* **2021**, *609*, No. 121195.
(31) Lombardo, D.; Kiselev, M. A. Methods of Liposomes Preparation: Formation and Control Factors of Versatile Nanocarriers for Biomedical and Nanomedicine Application. *Pharmaceutics* **2022**, *14* (3), No. 543, DOI: 10.3390/pharmaceutics14030543.
(32) Hassett, K. J.; Higgins, J.; Woods, A.; Levy, B.; Xia, Y.; Hsiao, C. J.; Acosta, E.; Almarsson, Ö.; Moore, M. J.; Brito, L. A. Impact of lipid nanoparticle size on mRNA vaccine immunogenicity. *J. Controlled Release* **2021**, *335*, 237−246.
(33) Niculescu, A.-G.; Bîrcă, A. C.; Grumezescu, A. M. New Applications of Lipid and Polymer-Based Nanoparticles for Nucleic Acids Delivery. *Pharmaceutics* **2021**, *13* (12), No. 2053, DOI: 10.3390/pharmaceutics13122053.
(34) Penacho, N.; Rosa, M.; Lindman, B.; Miguel, M. G.; Simões, S.; de Lima, M. C. P. Physicochemical properties of transferrin-associated lipopolyplexes and their role in biological activity. *Colloids Surf., B* **2010**, *76* (1), 207−214, DOI: 10.1016/j.colsurfb.2009.10.034.
(35) Jürgenliemk, G.; Nahrstedt, A. Dissolution, solubility and cooperativity of phenolic compounds from *Hypericum perforatum* L. in aqueous systems. *Pharmazie* **2003**, *58* (3), 200−203.
(36) de Morais, F. A.; Gonçalves, R. S.; Vilsinski, B. H.; de Oliveira, É. L.; Rocha, N. L.; Hioka, N.; Caetano, W. Hypericin photodynamic activity in DPPC liposome. PART I: biomimetism of loading, location, interactions and thermodynamic properties. *J. Photochem. Photobiol., B* **2019**, *190*, 118−127, DOI: 10.1016/j.jphotobiol.2018.11.019.
(37) Sardoiwala, M. N.; Kushwaha, A. C.; Dev, A.; Shrimali, N.; Guchhait, P.; Karmakar, S.; Roy Choudhury, S. Hypericin-Loaded Transferrin Nanoparticles Induce PP2A-Regulated BMI1 Degradation in Colorectal Cancer-Specific Chemo-Photodynamic Therapy. *ACS Biomater. Sci. Eng.* **2020**, *6* (5), 3139−3153.
(38) Arnida; Nishiyama, N.; Kanayama, N.; Jang, W.-D.; Yamasaki, Y.; Kataoka, K. PEGylated gene nanocarriers based on block catiomers bearing ethylenediamine repeating units directed to remarkable enhancement of photochemical transfection. *J. Controlled Release* **2006**, *115* (2), 208−215, DOI: 10.1016/j.jconrel.2006.07.014.
(39) Zarei, H.; Malaekeh-Nikouei, B.; Ramezani, M.; Soltani, F. Multifunctional peptides based on low molecular weight protamine (LMWP) in the structure of polyplexes and lipopolyplexes: Design, preparation and gene delivery characterization. *J. Drug Delivery Sci. Technol.* **2021**, *62*, No. 102422.
(40) Marxer, E. E. J.; Brüßler, J.; Becker, A.; Schümmelfeder, J.; Schubert, R.; Nimsky, C.; Bakowsky, U. Development and characterization of new nanoscaled ultrasound active lipid dispersions as contrast agents. *Eur. J. Pharm. Biopharm.* **2011**, *77* (3), 430−437.
(41) Xie, Y.; Kim, N. H.; Nadithe, V.; Schalk, D.; Thakur, A.; Kılıç, A.; Lum, L. G.; Bassett, D. J.; Merkel, O. M. Targeted delivery of siRNA to activated T cells via transferrin-polyethylenimine (Tf-PEI) as a potential therapy of asthma. *J. Controlled Release* **2016**, *229*, 120−129.
(42) Bofinger, R.; Zaw-Thin, M.; Mitchell, N. J.; Patrick, P. S.; Stowe, C.; Gomez-Ramirez, A.; Hailes, H. C.; Kalber, T. L.; Tabor, A. B. Development of lipopolyplexes for gene delivery: A comparison of the effects of differing modes of targeting peptide display on the structure and transfection activities of lipopolyplexes. *J. Pept. Sci.* **2018**, *24* (12), No. e3131.
(43) Rezaee, M.; Oskuee, R. K.; Nassirli, H.; Malaekeh-Nikouei, B. Progress in the development of lipopolyplexes as efficient non-viral gene delivery systems. *J. Controlled Release* **2016**, *236*, 1−14.
(44) Abdelsalam, A. M.; Somaida, A.; Ambreen, G.; Ayoub, A. M.; Tariq, I.; Engelhardt, K.; Garidel, P.; Fawaz, I.; Amin, M. U.; Wojcik, M.; Bakowsky, U. Surface tailored zein as a novel delivery system for hypericin: Application in photodynamic therapy. *Mater. Sci. Eng., C* **2021**, *129*, No. 112420.
(45) Shao, C.; Shang, K.; Xu, H.; Zhang, Y.; Pei, Z.; Pei, Y. Facile fabrication of hypericin-entrapped glyconanoparticles for targeted photodynamic therapy. *Int. J. Nanomed.* **2018**, *13*, 4319−4331, DOI: 10.2147/IJN.S161262.
(46) Liu, L.; Chen, Y.; Liu, C.; Yan, Y.; Yang, Z.; Chen, X.; Liu, G. Effect of Extracellular Matrix Coating on Cancer Cell Membrane-Encapsulated Polyethyleneimine/DNA Complexes for Efficient and Targeted DNA Delivery In Vitro. *Mol. Pharmaceutics* **2021**, *18* (7), 2803−2822, DOI: 10.1021/acs.molpharmaceut.1c00359.
(47) Lu, H.-L.; Syu, W.-J.; Nishiyama, N.; Kataoka, K.; Lai, P.-S. Dendrimer phthalocyanine-encapsulated polymeric micelle-mediated photochemical internalization extends the efficacy of photodynamic therapy and overcomes drug-resistance in vivo. *J. Controlled Release* **2011**, *155* (3), 458−464, DOI: 10.1016/j.jconrel.2011.06.005.
(48) Hellum, M.; Høgset, A.; Engesaeter, B. O.; Prasmickaite, L.; Stokke, T.; Wheeler, C.; Berg, K. Photochemically enhanced gene delivery with cationic lipid formulations. *Photochem. Photobiol. Sci.* **2003**, *2* (4), 407−411.
(49) Hall, A.; Lächelt, U.; Bartek, J.; Wagner, E.; Moghimi, S. M. Polyplex Evolution: Understanding Biology, Optimizing Performance. *Mol. Ther.* **2017**, *25* (7), 1476−1490.
(50) Gargouri, M.; Sapin, A.; Arıca-Yegin, B.; Merlin, J. L.; Becuwe, P.; Maincent, P. Photochemical internalization for pDNA transfection: evaluation of poly(d,l-lactide-co-glycolide) and poly(ethylenimine) nanoparticles. *Int. J. Pharm.* **2011**, *403* (1−2), 276−284, DOI: 10.1016/j.ijpharm.2010.10.040.
(51) Park, S.-j.; Na, K. The transfection efficiency of photosensitizer-induced gene delivery to human MSCs and internalization rates of EGFP and Runx2 genes. *Biomaterials* **2012**, *33* (27), 6485−6494.
(52) Oliveira, S.; Fretz, M. M.; Høgset, A.; Storm, G.; Schiffelers, R. M. Photochemical internalization enhances silencing of epidermal growth factor receptor through improved endosomal escape of siRNA. *Biochim. Biophys. Acta, Biomembr.* **2007**, *1768* (5), 1211−1217.
(53) Suzuki, I. L.; de Araujo, M. M.; Bagnato, V. S.; Bentley, M. V. L. B. TNFα siRNA delivery by nanoparticles and photochemical internalization for psoriasis topical therapy. *J. Controlled Release* **2021**, *338*, 316−329, DOI: 10.1016/j.jconrel.2021.08.039.
(54) Zhang, Q.; Kuang, G.; He, S.; Lu, H.; Cheng, Y.; Zhou, D.; Huang, Y. Photoactivatable Prodrug-Backboned Polymeric Nanoparticles for Efficient Light-Controlled Gene Delivery and Synergistic Treatment of Platinum-Resistant Ovarian Cancer. *Nano Lett.* **2020**, *20* (5), 3039−3049, DOI: 10.1021/acs.nanolett.9b04981.
(55) Chen, W.; Deng, W.; Xu, X.; Zhao, X.; Vo, J. N.; Anwer, A. G.; Williams, T. C.; Cui, H.; Goldys, E. M. Photoresponsive endosomal escape enhances gene delivery using liposome−polycation−DNA (LPD) nanovectors. *J. Mater. Chem. B* **2018**, *6* (32), 5269−5281.
(56) Chen, W.; Deng, W.; Goldys, E. M. Light-Triggerable Liposomes for Enhanced Endolysosomal Escape and Gene Silencing in PC12 Cells. *Mol. Ther. Nucleic Acids* **2017**, *7*, 366−377.
(57) Li, K.-T.; Duan, Q.-Q.; Chen, Q.; He, J.-W.; Tian, S.; Lin, H.-D.; Gao, Q.; Bai, D.-Q. The effect of aloe emodin−encapsulated nanoliposome-mediated r-caspase-3 gene transfection and photodynamic therapy on human gastric cancer cells. *Cancer Med.* **2016**, *5* (2), 361−369.
(58) de Ilarduya, C. T.; Sun, Y.; Düzgüneş, N. Gene delivery by lipoplexes and polyplexes. *Eur. J. Pharm. Sci.* **2010**, *40* (3), 159−170.
(59) Bendas, G.; Krause, A.; Bakowsky, U.; Vogel, J.; Rothe, U. Targetability of novel immunoliposomes prepared by a new antibody conjugation technique. *Int. J. Pharm.* **1999**, *181* (1), 79−93.
(60) Bakowsky, H.; Richter, T.; Kneuer, C.; Hoekstra, D.; Rothe, U.; Bendas, G.; Ehrhardt, C.; Bakowsky, U. Adhesion characteristics and stability assessment of lectin-modified liposomes for site-specific drug delivery. *Biochim. Biophys. Acta, Biomembr.* **2008**, *1778* (1), 242−249.
(61) Berstad, M. B.; Weyergang, A.; Berg, K. Photochemical internalization (PCI) of HER2-targeted toxins. *Biochim. Biophys. Acta, Gen. Subj.* **2012**, *1820* (12), 1849−1858.